Nonalcoholic fatty liver disease is associated with decreased hepatocyte mitochondrial respiration, but not mitochondrial number

Authors and affiliations: MC Sinton[1], J Meseguer Ripolles[2], B Lucendo Villarin[2], MJ Lyall[1], RN Carter[1], NM Morton[1], DC Hay[2], AJ Drake[1]

Corresponding author:

Amanda J. Drake: University/BHF Centre for Cardiovascular Science, Queen's Medical Research Institute, Edinburgh BioQuarter, 47 Little France Crescent, Edinburgh EH16 4TJ. mandy.drake@ed.ac.uk

Address:

1. University/BHF Centre for Cardiovascular Science, Queen's Medical Research Institute, Edinburgh BioQuarter, 47 Little France Crescent, Edinburgh EH16 4TJ

2. Scottish Centre for Regenerative Medicine, Edinburgh BioQuarter, 5 Little France Crescent, Edinburgh, EH16 4UU

Abstract

Nonalcoholic fatty liver disease (NAFLD) is currently the most prevalent form of liver disease worldwide. This term covers a spectrum of pathologies, from benign hepatic steatosis to non-alcoholic steatohepatitis (NASH). As the disease progresses, NASH can develop into cirrhosis and hepatocellular carcinoma. However, the underlying mechanisms and the factors which predispose an individual to disease progression remain poorly understood. Whilst NAFLD appears to be associated with mitochondrial dysfunction, it is unclear whether this is due to respiratory impairment, changes in mitochondrial mass, or mitochondrial fragmentation. Using a human pluripotent stem cell-based model of NAFLD we show that exposure to lactate, pyruvate and octanoic acid results in the development of macrovesicular steatosis. We do not observe changes in mitochondrial mass or fragmentation but do find decreases in maximal respiration and reserve capacity, suggesting impairment in the electron transport chain (ETC). Taken together, these findings indicate that the development of macrovesicular steatosis in NAFLD may be linked to the impairment of the ETC in mitochondria.

43 **Introduction**

44 Non-alcoholic fatty liver disease (NAFLD) is the most prevalent form of hepatic disease
45 globally, estimated to affect 1 in 3 people. It is closely related to obesity, with ~88% of obese
46 individuals at risk of developing the disease[1]. NAFLD is characterised by excess accumulation
47 of triglycerides (TGs) in hepatocytes, leading to the development of steatosis[2]. Steatotic
48 hepatocytes accumulate TGs in single large, or multiple medium-sized, cytoplasmic lipid
49 droplets[3] and whilst simple steatosis is largely benign, its presence increases the risk of
50 developing non-alcoholic steatohepatitis (NASH), which may progress to cirrhosis and
51 hepatocellular carcinoma[4]. It is unclear why only a subset of patients develop NASH and, other
52 than bariatric surgery for morbidly obese patients, there are currently no specific therapeutics
53 available to treat or reverse this pathology[5].

54

55 Multiple studies suggest that the pathology of NAFLD is linked to impairment of mitochondrial
56 function[6–9]. In rat models, mitochondrial dysfunction precedes the development of hepatic
57 steatosis, suggesting that disease pathology and progression are linked to impairment of
58 mitochondrial function[10]. NAFLD is linked to structural changes in mitochondrial cristae and
59 the development of crystalline inclusion bodies[11]. As electron transport chain (ETC)
60 components are embedded in the cristae, structural changes may have a physical impact on
61 respiration[12]. Similarly, the growth of inclusion bodies may also impair oxidative
62 phosphorylation and lead to increased free radical production[11]. This is supported by
63 observations of NAFLD-associated hepatic oxidative stress and altered levels of fatty acid
64 beta oxidation[11,12]. This is supported by the observation of NAFLD-associated hepatic
65 oxidative stress and altered levels of fatty acid beta oxidation[11,12]. Furthermore, in humans,
66 once hepatic lipid content exceeds 10%, lipid export is compromised[13]. In tandem with altered
67 fatty acid beta oxidation, this imbalance may lead to the accumulation of intracellular lipids
68 observed in NAFLD.

69 Satapati et al. (2012) observed increased tricarboxylic acid (TCA) cycle activity and
70 anaplerosis in the livers of mice with high fat diet-induced hepatic steatosis[7]. They also
71 demonstrate that increased levels of hepatic TGs induced oxidative metabolism, with a
72 proportional increase in oxidative stress[14]. Indirect studies in humans indicate a similar effect
73 on TCA cycle flux[6]. As TCA cycle flux generates NADH and $FADH_2$, which transfer electrons
74 to the electron transport chain (ETC), alterations in TCA cycling may have a direct impact on
75 respiration and oxidative stress. Further studies in humans demonstrate that NAFLD and
76 NASH are associated with increased and decreased mitochondrial maximal respiration,
77 respectively, indicating that there is a transition in mitochondrial function between these two
78 disease states[15]. The reasons for this are unclear; such differences in maximal respiration
79 between NAFLD and NASH could reflect impairment of the ETC and/or changes in baseline
80 mitochondrial respiration. Furthermore, mitochondria isolated from whole tissue come from
81 multiple cell types, which may differ in proportion in disease states and this may confound the
82 interpretation of any results. Observations that mitochondrial mass increased in NASH with a
83 concomitant decrease in maximal respiration may also arise from organelle fragmentation, a
84 phenotype associated with oxidative stress and apoptosis in other diseases[16].
85
86 In light of current knowledge, we hypothesised that nutrient excess in NAFLD leads to
87 mitochondrial dysfunction and subsequent increases in ETC activity due to increased
88 availability of respiratory substrates. Therefore, we aimed to determine the impact of lipid
89 accumulation on mitochondrial respiration specifically in hepatocytes, to avoid the
90 confounding effects associated with bulk tissue analysis. We also aimed to determine whether
91 changes in respiration were related to altered mitochondrial mass or fragmentation. To this
92 end, we used a recently developed *in vitro* model of NAFLD[17] to explore the impact of hepatic
93 steatosis on mitochondrial respiration.
94

Methods

Differentiation of pluripotent human stem cells to hepatocyte-like cells and induction of intracellular lipid accumulation

Human female H9 pluripotent stem cells (PSCs) were differentiated to hepatocyte-like cells (HLCs) as previously described[18]. HLCs were cultured in a 96-well format for measurements of lipid accumulation and in a 6-well format for all other analyses. Intracellular lipid accumulation was induced in HLCs, as previously described[17]. Briefly, at day 17, HLCs were exposed to a cocktail of sodium l-lactate (L; 10mM), sodium pyruvate (P; 1 mM) and octanoic acid (O; 2 mM) (Sigma, Gillingham, UK).

High content analysis microscopy

Cells were stained with a cell painter assay, adapted from Lyall *et al* and Bray *et al*[17,19]. Cells were fixed with 50 µL/well 4% (wt/vol) paraformaldehyde (Electron Microscopy Sciences, 15710-S) for 15 minutes at room temperature. For permeabilisation, cells were incubated in 0.1% Triton X-100 (Sigma-Aldrich, T8787) in PBS for 15 minutes at room temperature. For lipid droplet analysis, cells were then stained with a combination of NucBlue Live ReadyProbes® Reagent (2 drops/mL) (Molecular Probes, R37605), HCS CellMask™ Red (2 µL/10 mL) (Invitrogen, H32712), and BODIPY™ 493/503 (1:1000) (Life Sciences, D3922), as per the manufacturer's instructions. For mitochondrial quantification, cells were stained with a combination of NucBlue Live ReadyProbes® Reagent (2 drops/mL), MitoTracker™ Deep Red FM (1/4000; Invitrogen, M22426), and Alexa Fluor™ 555 Phalloidin (Invitrogen, A34055). Following staining, images were acquired using an Operetta High Content Analysis microscope (Perkin Elmer, Buckinghamshire, UK). Lipid droplet morphology was analysed as previously described[17].

121 **Cell mitochondrial stress test assay**

122 The oxygen consumption rate (OCR) of LPO-exposed HLCs was measured using the Agilent
123 Seahorse XF Cell Mito Stress Test Kit (Agilent, 103015-100) on a Seahorse XF Analyser
124 (Agilent, California, USA). Analysis was performed under basal conditions, and following
125 treatment with oligomycin A (an ATPase inhibitor), carbonyl-cyanide-4-(trifluoromethoxy)
126 phenylhydrazone (FCCP; an ETC uncoupler), and combined rotenone and antimycin A
127 (inhibitors of complex I and III, respectively). Two concentrations of FCCP (0.5 µM and 1.0
128 µM) were used for optimisation. Since replicates within each group responded similarly to
129 each other, results were combined. OCR was normalised to total protein for each well, using
130 the sulforhodamine B (SRB) assay, as previously described[20], but with spectrophotometric
131 measurements read at 540 nm.

132

133 **Citrate synthase assay**

134 Mitochondria were isolated using the Mitochondria Isolation Kit for Cultured Cells (Thermo
135 Scientific, 89874), as per the manufacturer's instructions, selecting option A for isolation.
136 Citrate synthase activity, a marker for mitochondrial integrity, was then measured using the
137 Citrate Synthase Activity Colorimetric Assay Kit (BioVision, K318), as per the manufacturer's
138 instructions.

139

140 **Protein Extraction**

141 Adherent HLCs were washed once with ice-cold PBS, before incubating in ice-cold RIPA Lysis
142 and Extraction Buffer (Thermo Scientific, 89900) supplemented with cOmplete™ Protease
143 Inhibitor Cocktail tablets (1/10 mL buffer; Roche, 11697498001). The suspended HLCs were
144 placed on ice for 30 minutes, vortexing every 3 minutes, before centrifuging for 20 min at 4
145 °C, 12,000 rpm. The supernatant was collected and stored at -80 °C until needed.

146

147 **Western blot analysis**

148 Protein quantification was performed using the Qubit™ Protein Assay Kit (Invitrogen, Q33211),
149 as per the manufacturer's instructions. Protein concentration was measured using a Qubit™
150 Fluorometer (Invitrogen, Massachusetts, USA). Equal concentrations (50 µg) of HLC protein
151 extract in 4 x Sample Loading Buffer (Li-Cor, 928-40004) were loaded onto NuPAGE™ 4-12%
152 Bis-Tris Protein Gels (Invitrogen, NP0326BOX). Following resolution, protein was transferred
153 to a methanol-activated polyvinylidene difluoride (PVDF) membrane. Protein transfer was
154 measured using Revert 700 Total Protein Stain Kit (Li-Cor, 926-11010) as per the
155 manufacturer's instructions. Membranes were then blocked with Tris-buffered saline
156 containing Tween 20 (TBST) and 5% skimmed milk powder, before incubating with either
157 Pyruvate Dehydrogenase (C54G1) Rabbit mAb (Cell Signaling Technology, 3205) or SDHA
158 (D6J9M) XP® Rabbit mAb (Cell Signaling Technology, 11998), both a 1:1000 dilution. The
159 membranes were washed in TBST before incubating with the secondary antibody, IRDye®
160 680RD Donkey anti-Mouse IgG (Li-Cor, 926-68072) at a 1:10,000 dilution, for 1 h at room
161 temperature, in the dark, with shaking. Blots were visualised on a Li-Cor Odyssey® CLx (Li-
162 Cor, Nebraska, USA), and bands normalised to the Revert 700 Total Protein Stain, as per the
163 manufacturer's instructions.

164

165 **Real-time quantitative PCR**

166 Total RNA was extracted from HLCs using the Monarch® Total RNA Miniprep Kit (New
167 England BioLabs, T2010). cDNA was generated using the High Capacity cDNA Reverse
168 Transcriptase Kit (Applied Biosystems, 4368814). A master mix was prepared using PerfeCTa
169 FastMix II (Quanta Biosciences, Inc., 95118-250). cDNA was amplified and quantified using
170 the Universal Probe Library (Roche, Burgess Hill, UK) system on a Roche LightCycler 480
171 (Roche Diagnostics Ltd, Switzerland). Details of primers and Universal Probe Library probes
172 (Roche) and primers used can be found in Table S1.

173 **Measurement of mitochondrial and nuclear DNA**

174 DNA was extracted from HLCs using the Monarch® Genomic DNA Purification Kit (New
175 England BioLabs, T3010). A master mix was prepared using the Luna® Universal qPCR
176 Master Mix (New England BioLabs, M3003). DNA was amplified and quantified using a Roche
177 LightCycler 480 (Roche Diagnostics Ltd, Switzerland). Primers were designed against two
178 regions of the NCBI mitochondrial reference sequence NC_012920.1, and one region of the
179 genomic reference sequence NC_000011.10. Primers used can be found in Table S2.

180

181 **Statistical analyses**

182 All statistical analyses were performed using Graph Prism Version 8.0 for Windows or macOS,
183 GraphPad Software, La Jolla California USA, www.graphpad.com. Normality of data
184 distribution was measured using the Shapiro-Wilks test. Normally distributed data were
185 analysed using a parametric unpaired Student's t-test, and non-normally distributed data were
186 analysed using a non-parametric Mann-Whitney test. Data were considered to be significant
187 where $p < 0.05$.

188

189 **Results**

190 **LPO-treatment induces macrovesicular steatosis in HLCs**

191 We previously reported that the high energy substrate cocktail LPO promotes intracellular lipid
192 accumulation in HLCs[17] although it was not known whether LPO promotes lipid droplet
193 biogenesis or increased accumulation of lipids within existing droplets. Stem cell derived HLCs
194 were differentiated and characterised as before[18] (Figure 1A). Analysis of gene expression
195 using RT-qPCR showed increased expression of transcripts for PLIN2, PLIN4, and PLIN5,
196 which are typically associated with intracellular lipid droplet membranes, suggesting an
197 increase in lipid droplet size (Figure 1B-D). Analysis of lipid accumulation using high content
198 imaging (Figure 1E) demonstrated that LPO exposure was not associated with a change in
199 the number of lipid droplets (Figure 1F), but led to a ~2-fold increase in the size of intracellular
200 lipid droplets (Figure 1G), consistent with the development of macrovesicular steatosis.

201

202 **Macrovesicular steatosis in hepatocytes is associated with electron transport chain**
203 **dysfunction**

204 It has been suggested that NAFLD-associated macrovesicular steatosis results in impairment
205 of mitochondrial respiration and we therefore proceeded to analyse this in steatotic HLCs
206 (Figure 2A). Basal oxygen consumption rate (OCR), representing combined mitochondrial and
207 non-mitochondrial oxygen consumption, was unchanged following LPO exposure (Figure 2B).
208 Additionally, oligomycin A, a complex V inhibitor decreased OCR equally effectively in control
209 and treatment group. Firstly, this indicated that there were no changes in ATP-linked
210 respiration in response to macrovesicular steatosis (Figure 2C). Secondly, when comparing
211 oligomycin A-induced alterations in OCR with those following addition of rotenone/antimycin
212 A, we could detect no changes in proton leak between groups (Figure 2D). The addition of the
213 ETC uncoupler FCCP revealed a decrease in maximal respiration in the steatotic HLCs,
214 suggesting ETC dysfunction (Figure 2E). Using OCR measurements following FCCP

215 treatment, and comparing to the basal OCR, we calculated that there was a decrease in
216 reserve capacity in the LPO-treated cells, compared with controls (Figure 2F). Subsequently,
217 complex I and III were targeted with rotenone/antimycin A, to completely inhibit oxidative
218 phosphorylation, which reduced OCR to a similar level in both groups, suggesting no
219 difference in non-mitochondrial sources of OCR between the control and steatotic HLCs.
220

221 **Induction of macrovesicular steatosis is not associated with mitochondrial**
222 **fragmentation or alterations in mitochondrial number**

223 To analyse whether the observed changes in OCR could be due to mitochondrial
224 fragmentation rather than ETC dysfunction we measured citrate synthase (CS) activity. LPO
225 treatment had no impact on CS activity (Figure 3A), suggesting that mitochondria remain intact
226 following intracellular lipid accumulation. A final question was whether changes in ETC
227 function, as demonstrated by decreased cellular maximal respiration and reserve capacity,
228 were due to decreased numbers of mitochondria in response to intracellular lipid
229 accumulation. Since these were the only respiratory measurements to change, we
230 hypothesised that this was not the case. We first measured protein levels of succinate
231 dehydrogenase subunit A (SDHA) and pyruvate dehydrogenase (PDH) (Figure 3B), which
232 localise to the mitochondria. Protein levels of SDHA and PDH did not change in response to
233 intracellular lipid accumulation, suggesting that mitochondrial number is not altered by LPO-
234 induced macrovesicular steatosis. Furthermore, there were no changes in mitochondrial or
235 nuclear DNA (Figure 3C) and no change in the ratio of nuclear to mitochondrial DNA (Figure
236 3D). Finally, we used a high content microscopy-based approach to measure intracellular
237 mitochondrial quantity (Figure 3E), and observed no changes following exposure to LPO
238 (Figure 3F). Taken together, these data suggest that mitochondrial number is not altered in
239 the presence of intracellular lipid accumulation.
240

241 **Discussion**

242 In this study we aimed to determine the nature of NAFLD-associated changes in mitochondrial
243 respiration, and whether these occur as a result of mitochondrial dysfunction or reductions in
244 mitochondrial number. Using a combination of high content microscopy and gene expression
245 analyses, we first confirmed that treatment of HLCs with LPO induced intracellular lipid
246 accumulation (Figure 1). The observed changes in the expression of genes associated with
247 lipid droplet size (PLIN2, 4 and 5) are also in agreement with findings from human studies with
248 intracellular lipid accumulation associated with an upregulation of PLIN2 in human
249 hepatocytes[21] and biopsies[19] from NAFLD patients. In adipocytes, PLIN4 localises to the
250 surface of unilocular lipid droplets, and may participate in their early development. Although
251 there are no human studies describing perturbed expression of PLIN4 in association with
252 NAFLD, its knockout protects against liver steatosis in mice[22]. Furthermore, PLIN4 knockout
253 diminishes the accumulation of triacylglycerol in lipid droplets and reduces the expression of
254 PLIN5 in mouse cardiac tissue. Therefore, their interplay may be important for the pathology
255 of NAFLD. In support of this, *in vitro* studies show that PLIN5 blocks lipid droplet lipolysis in
256 hepatocytes and an increase in PLIN5 expression may therefore contribute to the
257 development of macrovesicular steatosis[23]. Increases in the expression of PLIN2, PLIN4 and
258 PLIN5 in LPO-treated HLCs, alongside BODIPY staining, strongly indicate that this model
259 recapitulates macrovesicular steatosis observed in humans with NAFLD.

260

261 Following the further establishment of relevance to human disease, we wished to understand
262 whether macrovesicular steatosis was linked to dysfunction of mitochondrial respiration[15].
263 Previous studies have shown that mitochondrial maximal respiration increases in obese
264 humans with NAFLD but decreases on progression to NASH, despite an increase in
265 mitochondrial mass. In contrast to the initial hypothesis, we observed decreased maximal
266 respiration and reserve capacity in cells displaying a NAFLD phenotype. This indicates that

267 whilst mitochondria are mostly able to maintain respiratory integrity in LPO-exposed cells, the
268 ETC, and therefore oxidative phosphorylation, may be compromised. Given that these were
269 the only parameters of mitochondrial respiration to change, it suggests that LPO treatment of
270 HLCs inhibits complexes I-III of the ETC. This effect may arise due to the use of octanoic acid,
271 which inhibits complex I-III in rat liver, as well as increasing oxidative stress through reactive
272 oxygen species production[24]. Inhibition of complex II may also impact on the TCA cycle,
273 potentially altering its function, and the generation of cofactors necessary for oxidative
274 phosphorylation, further impacting on cellular metabolism. However, further studies are
275 required to test these hypotheses.
276
277 Finally, we questioned whether changes in maximal respiration arose from fragmentation of
278 mitochondria or resulted from increased biogenesis. Given that maximal respiration was the
279 only parameter of respiration that changed, we suspected this was not the case. This was
280 confirmed by lack of change in the ratio of nuclear to mitochondrial DNA, suggesting that
281 mitochondrial biogenesis was not affected by LPO treatment in these studies. This is
282 consistent with human studies of NAFLD which show no changes in mitochondrial mass in
283 steatotic versus non-steatotic liver tissue[15]. In contrast, liver tissue from patients with NASH
284 contains greater numbers of mitochondria, with a concomitant decrease in maximal
285 respiration. Therefore, the model of NAFLD presented here may mirror the transition between
286 NAFLD and NASH, with respiratory dysfunction in the absence of mitochondrial biogenesis.
287 This discrepancy may also be due to previous studies using isolated mitochondria from whole
288 tissues, comprised of multiple cell types, whereas we examined a single cell population.
289
290 In conclusion, here we demonstrate that the treatment of HLCs with LPO induces intracellular
291 lipid accumulation in patterns similar to those observed in human pathology. Furthermore, we
292 observed decreased mitochondrial maximal respiration, in the absence of altered

293 mitochondrial biogenesis. Taken together, our data demonstrate that hepatocyte intracellular
294 lipid accumulation is linked to mitochondrial dysfunction in response to the changing
295 bioenergetic demands associated with NAFLD, impacting on the ETC, and limiting maximal
296 respiration.
297

Acknowledgements

MCS was supported by a British Heart Foundation PhD studentship and by the BHF Centre of Research Excellence. DCH, BLV were supported by an award from the Chief Scientist Office (TCS/16/37). JMR was supported by an MRC PhD studentship. We thank Will Cawthorn for discussions about mitochondrial quantification.

Author contributions

MCS, JMR, BLV, MJL, RNC and NMM performed experiments. DCH and AJD conceived the experiments. MCS, NMM, DCH and AJD wrote the paper. All authors contributed to drafts of the paper and approved the final version.

Declaration of Interests

Professor David C Hay is a co-founder, shareholder and director of Stemnovate Limited

312 **Figure Legends**

313 Figure 1. LPO treatment induces development of macrovesicular lipid droplets. (**A**) H9 hPSCs
314 differentiate to HLCs, losing pluripotency and gaining expression of the hepatic markers
315 albumin and HNF4A (n = 3 biological replicates/group); (**B-D**) PLIN2, PLIN4, and PLIN5
316 expression increases in response to LPO treatment (n = 3 biological replicates per group). (**E**)
317 Representative images of lipid accumulation in control & LPO-treated groups 10x
318 magnification. (**F**) Number of lipid droplets do not increase, (**G**) but intracellular lipid droplets
319 increase in size (n = 32 biological replicates/group). Data analysed using two-tailed Student t-
320 test and expressed as mean ± SD, *p<0.05, ****p<0.0001.

321

322 Figure 2. LPO treatment results in decreased maximal respiration in mitochondria but not in
323 other aspects of oxygen consumption rate. HLCs were injected sequentially from ports A-C
324 with 4 μM oligomycin, 0.5-1 μM FCCP, and 1 μM antimycin combined with 200 nM rotenone.
325 (**A**) Raw trace of OCR comparing cells with or without LPO treatment; (**B**) basal respiration;
326 (**C**) ATP-linked respiration; (**D**) proton leak; (**E**) maximal respiration; (**F**) reserve capacity
327 compared to control treatment (n = 18 and 16 biological replicates in the control and treatment
328 group, respectively). Data analysed using two-tailed Student t-test for parametric data, or
329 Mann-Whitney U test for non-parametric data, and expressed as mean ± SD.

330

331 Figure 3. LPO does treatment does induce mitochondrial fragmentation or change
332 mitochondrial number. (**A**) Levels of citrate synthase activity were unaltered by LPO treatment
333 (n = 3 biological replicates/group); (**B**) Protein levels of succinate dehydrogenase subunit A
334 (SDHA) and pyruvate dehydrogenase were unchanged (n = 6 biological replicates/group); (**C**)
335 no changes were observed in abundance of DNA in mitochondrial region 2 (MT2);
336 mitochondrial region 3 (MT3); or genomic region beta-globin (HBB); (**D**) there were no
337 significant changes in the ratio of mitochondrial to genomic DNA, indicating no alterations in

338 the quantity of mitochondria in response to treatment (n=4 biological replicates/group for **C**
339 and **D**); (**E**) Representative images of mitochondrial content in control & LPO-treated groups
340 10x magnification. Blue staining = NucBlue, red staining = MitoTracker Deep Red; (**F**) high
341 content microscopy revealed no changes in mitochondrial quantity in response to treatment
342 (n = 4 and 6 biological replicates in the control and treatment group, respectively). Data
343 analysed using two-tailed Student t-test for parametric data, or Mann-Whitney U test for non-
344 parametric data, and expressed as mean ± SD.
345
346 **Supplementary materials S1**.
347 Primer sequences and UPL probes used for qPCR assays

348 **References**

349 1. World Health Organization. Obesity and overweight. (2018). Available at:
350 https://www.who.int/news-room/fact-sheets/detail/obesity-and-overweight.

351 2. Valenti, L., Bugianesi, E., Pajvani, U. & Targher, G. Nonalcoholic fatty liver disease:
352 cause or consequence of type 2 diabetes? *Liver International* **36**, 1563–1579 (2016).

353 3. Wang, L. & Yu, S. Pathology of Non-Alcoholic Fatty Liver Disease. *Int. J. Dig. Dis.* **2**,
354 (2016).

355 4. Asrih, M. & Jornayvaz, F. R. Metabolic syndrome and nonalcoholic fatty liver disease:
356 Is insulin resistance the link? *Molecular and Cellular Endocrinology* **418**, 55–65 (2015).

357 5. Laursen, T. L. *et al.* Bariatric surgery in patients with non-alcoholic fatty liver disease -
358 From pathophysiology to clinical effects. *World Journal of Hepatology* **11**, 138–249
359 (2019).

360 6. Sunny, N. E., Parks, E. J., Browning, J. D. & Burgess, S. C. Excessive hepatic
361 mitochondrial TCA cycle and gluconeogenesis in humans with nonalcoholic fatty liver
362 disease. *Cell Metab.* **14**, 804–810 (2011).

363 7. Satapati, S. *et al.* Elevated TCA cycle function in the pathology of diet-induced hepatic
364 insulin resistance and fatty liver. *J. Lipid Res.* **53**, 1080–1092 (2012).

365 8. Patterson, R. E. *et al.* Lipotoxicity in steatohepatitis occurs despite an increase in
366 tricarboxylic acid cycle activity. *Am. J. Physiol. - Endocrinol. Metab.* **310**,
367 ajpendo.00492.2015 (2016).

368 9. Sunny, N. E., Bril, F. & Cusi, K. Mitochondrial Adaptation in Nonalcoholic Fatty Liver
369 Disease: Novel Mechanisms and Treatment Strategies. *Trends Endocrinol. Metab.* **28**,
370 250–260 (2017).

371 10. Rector, R. S. *et al.* Mitochondrial dysfunction precedes insulin resistance and hepatic
372 steatosis and contributes to the natural history of non-alcoholic fatty liver disease in an
373 obese rodent model. *J. Hepatol.* **52**, 727–736 (2010).

374 11. Sanyal, A. J. *et al.* Nonalcoholic steatohepatitis: Association of insulin resistance and
375 mitochondrial abnormalities. *Gastroenterology* **120**, 1183–1192 (2001).
376 12. Caldwell, S. H. *et al.* Mitochondrial abnormalities in non-alcoholic steatohepatitis. *J.*
377 *Hepatol.* **31**, 430–434 (1999).
378 13. Fabbrini, E. *et al.* Alterations in adipose tissue and hepatic lipid kinetics in obese men
379 and women with nonalcoholic fatty liver disease. *Gastroenterology* **134**, 424–431
380 (2008).
381 14. Satapati, S. *et al.* Mitochondrial metabolism mediates oxidative stress and inflammation
382 in fatty liver. *J. Clin. Invest.* **125**, 4447–4462 (2015).
383 15. Koliaki, C. *et al.* Adaptation of Hepatic Mitochondrial Function in Humans with Non-
384 Alcoholic Fatty Liver Is Lost in Steatohepatitis. *Cell Metab.* **21**, 739–746 (2015).
385 16. Knott, A. B., Perkins, G., Schwarzenbacher, R. & Bossy-Wetzel, E. Mitochondrial
386 fragmentation in neurodegeneration. *Nature Reviews Neuroscience* **9**, 505–518 (2008).
387 17. Lyall, M. J. *et al.* Modelling non-alcoholic fatty liver disease in human hepatocyte-like
388 cells. *Philos. Trans. R. Soc. B Biol. Sci.* **373**, 20170362 (2018).
389 18. Wang, Y. *et al.* Defined and Scalable Generation of Hepatocyte-like Cells from Human
390 Pluripotent Stem Cells. *J. Vis. Exp.* e55355–e55355 (2017).
391 19. Bray, M. A. *et al.* Cell Painting, a high-content image-based assay for morphological
392 profiling using multiplexed fluorescent dyes. *Nat. Protoc.* **11**, 1757–1774 (2016).
393 20. Orellana, E. & Kasinski, A. Sulforhodamine B (SRB) Assay in Cell Culture to Investigate
394 Cell Proliferation. *Bio-Protocol* **6**, (2016).
395 21. Sahini, N. & Borlak, J. Genomics of human fatty liver disease reveal mechanistically
396 linked lipid droplet–associated gene regulations in bland steatosis and nonalcoholic
397 steatohepatitis. *Transl. Res.* **177**, 41–69 (2016).
398 22. Chen, W. *et al.* Inactivation of Plin4 downregulates Plin5 and reduces cardiac lipid
399 accumulation in mice. *Am. J. Physiol. - Endocrinol. Metab.* **304**, E770-9 (2013).

23. Wang, C. *et al.* Perilipin 5 improves hepatic lipotoxicity by inhibiting lipolysis. *Hepatology* **61**, 870–882 (2015).

24. Scaini, G. *et al.* Toxicity of octanoate and decanoate in rat peripheral tissues: evidence of bioenergetic dysfunction and oxidative damage induction in liver and skeletal muscle. *Mol. Cell. Biochem.* **361**, 329–335 (2012).

Figure 1

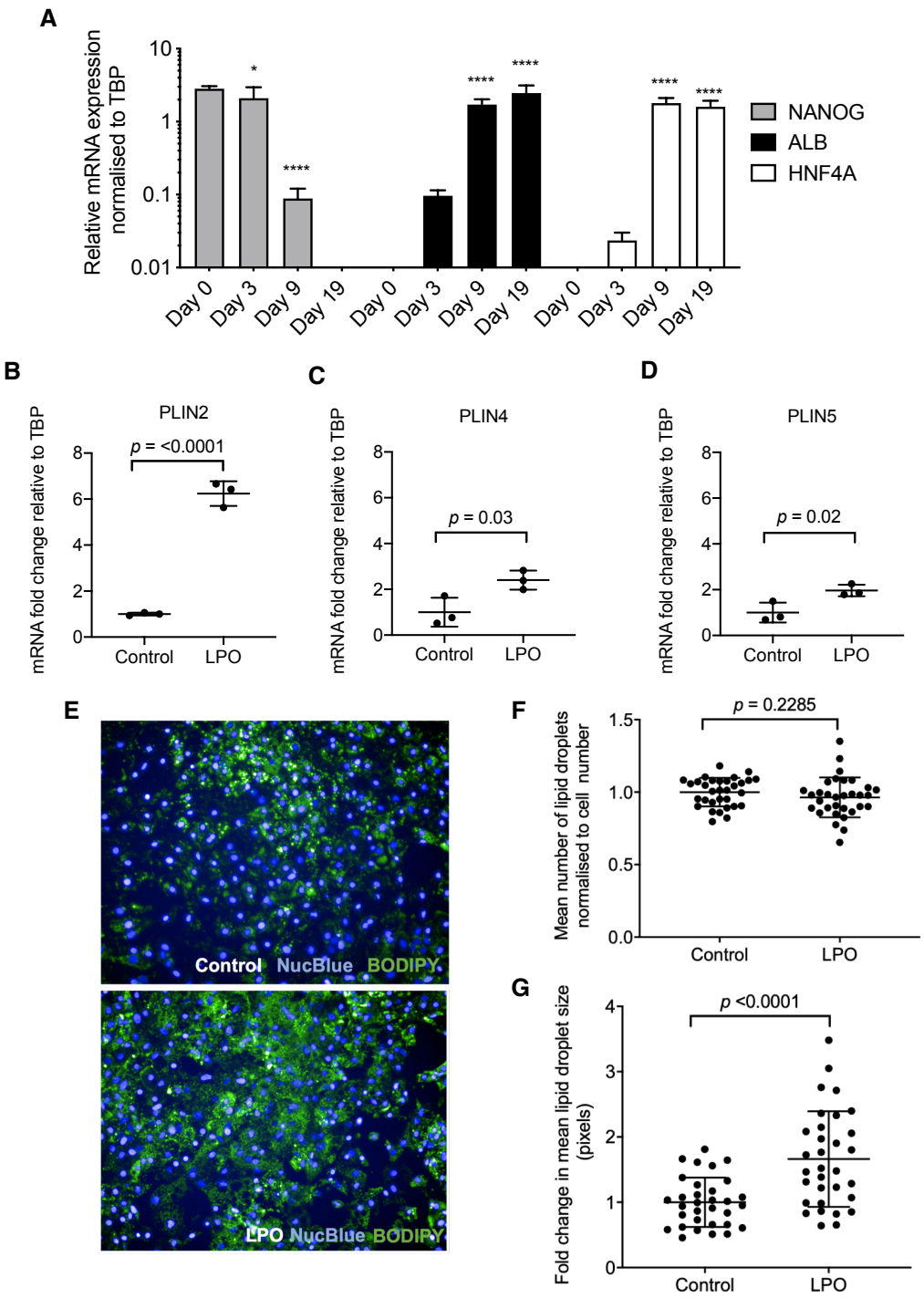
A
Relative mRNA expression normalised to TBP
10
1
0.1
0.01
*
****
****
****
****
****
NANOG
ALB
HNF4A
Day 0
Day 3
Day 9
Day 19
Day 0
Day 3
Day 9
Day 19
Day 0
Day 3
Day 9
Day 19
B
PLIN2
p = <0.0001
mRNA fold change relative to TBP
Control
LPO
C
PLIN4
p = 0.03
mRNA fold change relative to TBP
Control
LPO
D
PLIN5
p = 0.02
mRNA fold change relative to TBP
Control
LPO
E
Control NucBlue BODIPY
LPO NucBlue BODIPY
F
p = 0.2285
Mean number of lipid droplets normalised to cell number
Control
LPO
G
p <0.0001
Fold change in mean lipid droplet size (pixels)
Control
LPO

424

Figure 2

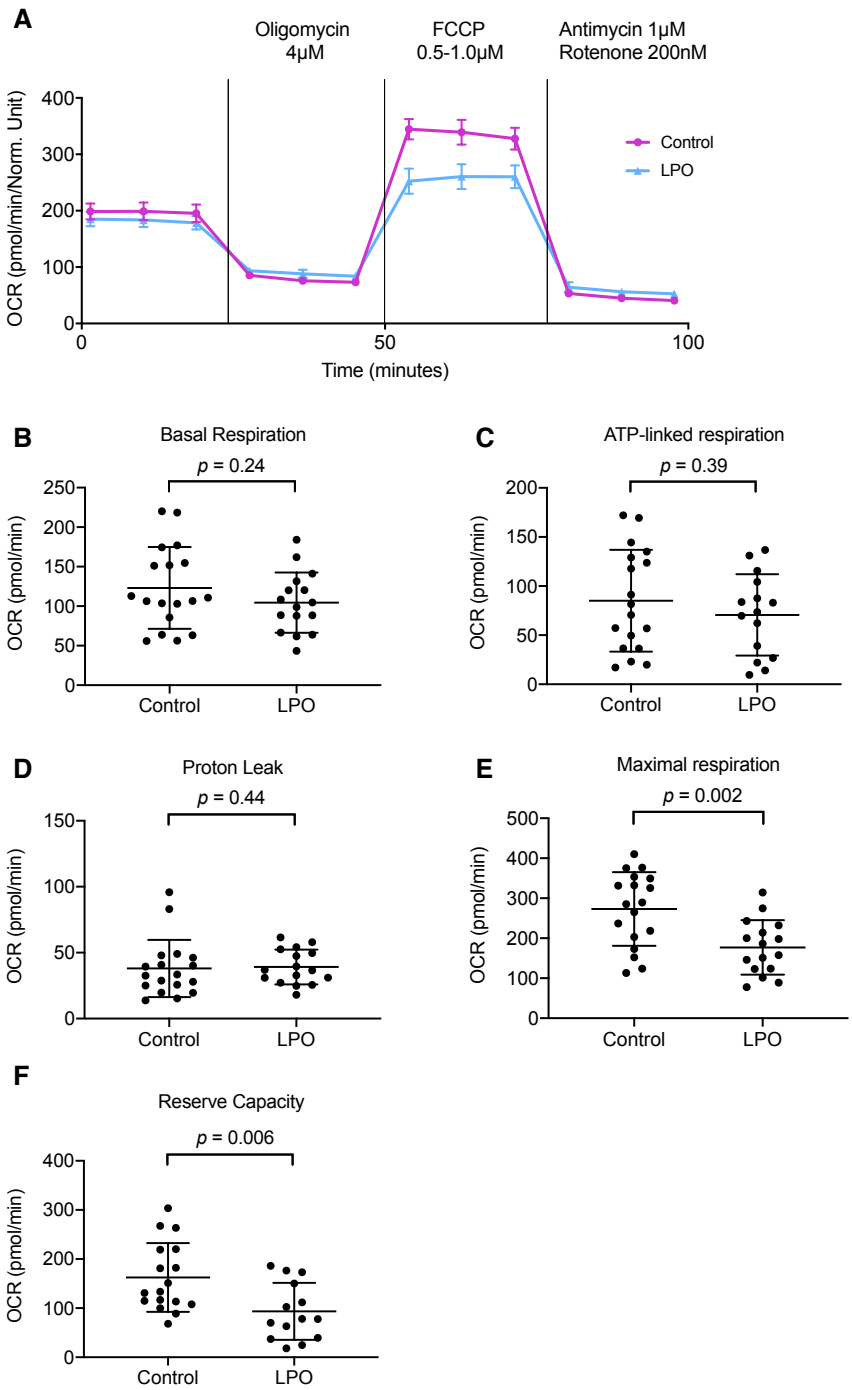
A
Oligomycin
4μM
FCCP
0.5-1.0μM
Antimycin 1μM
Rotenone 200nM
OCR (pmol/min/Norm. Unit)
Time (minutes)
Control
LPO
B
Basal Respiration
p = 0.24
OCR (pmol/min)
Control
LPO
C
ATP-linked respiration
p = 0.39
OCR (pmol/min)
Control
LPO
D
Proton Leak
p = 0.44
OCR (pmol/min)
Control
LPO
E
Maximal respiration
p = 0.002
OCR (pmol/min)
Control
LPO
F
Reserve Capacity
p = 0.006
OCR (pmol/min)
Control
LPO

425

Figure 3

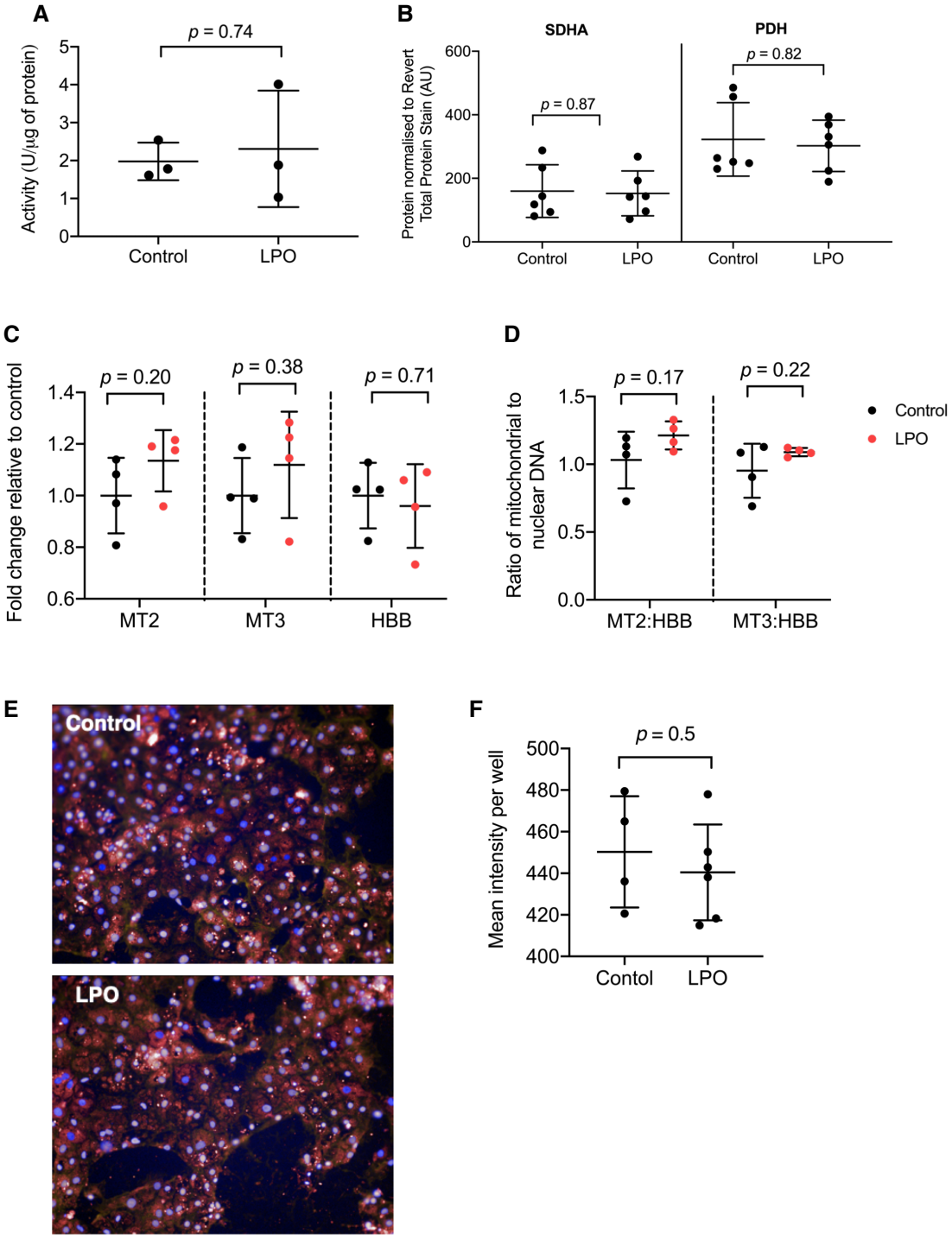
A
p = 0.74
Activity (U/µg of protein)
5
4
3
2
1
0
Control
LPO
B
SDHA
PDH
p = 0.87
p = 0.82
Protein normalised to Revert Total Protein Stain (AU)
600
400
200
0
Control
LPO
Control
LPO
C
p = 0.20
p = 0.38
p = 0.71
Fold change relative to control
1.4
1.2
1.0
0.8
0.6
MT2
MT3
HBB
D
p = 0.17
p = 0.22
Ratio of mitochondrial to nuclear DNA
1.5
1.0
0.5
0.0
MT2:HBB
MT3:HBB
Control
LPO
E
Control
LPO
F
p = 0.5
Mean intensity per well
500
480
460
440
420
400
Contol
LPO

426